Article

Thermodynamic and Kinetic Calculation of High Strength Aluminum-Lithium Alloy

Jinsan Wang [1],* and Xiang Xiao [2]

[1] AECC Beijing Institute of Aeronautical Materials, Huanshan Village, Wenquan Town, Haidian District, Beijing 100095, China

[2] Chinalco Materials & Application Research Institute, Beijing 102209, China; xiaoxiang_zhl@163.com

* Correspondence: wjsbiam@163.com

Abstract: High strength Al-Li alloy is the research focus of aluminum alloy. In the present paper, high strength Al-Li alloy 2A97 composed of Al-Li-Cu-Zn-Mg-Mn-Zr system is studied by thermodynamic and kinetic calculation. The equilibrium phase diagram and the metastable phases of 2A97 were calculated by thermodynamic method. The solidification phase diagram of 2A97 was obtained using the Scheil–Gulliver model. The continuous cooling transformation diagram and isothermal aging curves were calculated using the kinetic method. In addition, the 2A97 microstructures of cast, homogenized, hot-rolled, and solid solution were observed by a scanning electron microscope. The results can be used for the process optimization and microstructure control of 2A97. In particular, the research results of this work can be used for the determination of the homogenization temperature and solid-solution temperature.

Keywords: high strength Al-Li alloy; phase diagram; thermodynamic; kinetic

1. Introduction

In the field of aeronautics, the reduction in weight can improve the performance of aircraft. Al-Li alloys are considered to be potential lightweight and high-strength structural materials because of their low density, high strength and toughness, high specific modulus, appropriate rigidity and corrosion resistance [1–3]. Alcoa Company developed the first generation of Al-Li alloy. Its weight reduction effect is obvious, but its plasticity and toughness are too low. Therefore, researchers have developed second-generation Al-Li alloys having low density, medium strength, damage resistance and high specific strength [4,5]. However, it has many problems, such as high anisotropy of mechanical properties, low fracture toughness, poor corrosion resistance and difficult processing. In recent years, experts have successfully developed the third-generation Al-Li alloy with excellent comprehensive properties by adjusting the content of main alloy and microalloy elements. Among these, 2A97 Al-Li alloy is a new type of alloy independently developed in China [6–8]. This alloy has high strength, good welding performance and good processing performance [9–11].

The properties of Al-Li alloys are closely related to their microstructures [12,13], and the microstructure is determined by the composition and process of the alloy. 2A97 alloy is composed of an Al-Li-Cu-Zn-Mg-Mn-Zr system. Among these elements, the main alloying elements of 2A97 are Cu and Li, which precipitate strengthening phases T1-Al2CuLi, δ'-Al3Li and θ'-Al2Cu in the matrix. The microalloying elements of Zn, Mg, Mn and Zr are added in order to improve the overall performance. In addition, impurity elements Fe and Si inevitably appear in the alloy. The heat treatment process of 2A97 alloy mainly includes homogenization, solid-solution treatment and aging. Homogenization can eliminate the coarse non-equilibrium eutectic structure and dendrite segregation, thus improving the workability of the alloy. The purpose of solid-solution treatment is to dissolve solute elements in Al matrix at high temperature and form a supersaturated solid solution under

rapid cooling. The strengthening phases T1-Al2CuLi, δ'-Al3Li andθ'-Al2Cu are formed by subsequent aging [14–16]. Therefore, the process parameters of homogenization, solution treatment and aging have an important influence on the alloy properties.

Thermodynamic calculations can be used to acquire equilibrium, solidification and metastable phase diagrams. Kinetic calculations can be coupled with the thermodynamic data to obtain the continuous cooling transformation (CCT) and aging curves. The calculated results can predict the microstructure of the alloy at different temperatures and times, and provide theoretical guidance for the formulation of homogenization, solid-solution and aging processes. Chen [17] calculated the equilibrium phase diagram of Al-Li-Mg-Si alloy by the thermodynamic method, and determined the aging temperature as 170 °C to obtain δ'-Al3Li and Mg2Si precipitates. Deschamps [18] studied the precipitation process of Al-Li-Mg alloy during aging by the kinetic method, and obtained the formation temperature and time of δ'-Al3Li phase. However, there is no report on the thermodynamic and kinetic calculation in 2A97 alloy at present, and previous research work on the 2A97 alloy has mainly focused on the testing of the microstructure and mechanical properties.

In this study, thermodynamic and kinetic calculations of 2A97 Al-Li alloy were systematically implemented. The calculated results can be used for the process optimization and microstructure control of 2A97 [19,20].

2. Materials and Methodology

2.1. Thermodynamic Method of Calphad

The Computer Coupled Phase Diagram and Thermochemistry (CALPHAD) technique aims to promote thermodynamics calculation by developing models representing the thermodynamic properties of alloy phases. The thermodynamic model is described by the Gibbs energy function and can be used to calculate the phase diagram and material properties of alloy systems. In particular, the CALPHAD method may be used to effectively extrapolate phase diagrams of multicomponent alloy systems.

Thermodynamic models for the Gibbs energy of substitutional phase in a multicomponent system can be represented by the equation:

$$G = \sum_i x_i G_i^0 + RT \sum_i x_i \ln x_i + \sum_i \sum_j x_i x_j \sum_v \Omega_v (x_i - x_j)^v \tag{1}$$

where x_i is the mole fraction of component i, G_i^0 is the Gibbs energy of the phase in the pure component i, T is the temperature and R is the gas constant. Ω_v is an interaction coefficient dependent on the value of v.

The calculation of solidification is achieved by the implementation of the Scheil–Gulliver (SG) model. The model assumes that solute diffusion in the solid phase is slow enough to be considered negligible and that diffusion in the liquid is fast enough to assume that diffusion is complete. Therefore, the composition of solid formed during solidification (C_s), as a function of the fraction of solid formed (f_s), can be expressed as:

$$C_s = kC_0(1 - f_s)^{k-1} \tag{2}$$

where C_0 is the composition of the alloy and k is the partition coefficient. From this the fraction solid formed as a function of temperature is given by:

$$f_s = 1 - \left(\frac{T_f - T}{T_f - T_L} \right)^{\left(\frac{1}{k-1} \right)} \tag{3}$$

where T_L and T_f are the liquidus and solidus temperature.

By combining thermodynamic calculations based on the CALPHAD method and the SG model, solidification calculations can be carried out very quickly.

2.2. Kinetic Method

The evolution of the volume fraction during solid-state transformation can be described using the well-known Johnson–Mehl–Avrami (JMA) Equation [21]. Under isothermal conditions, it can be expressed as:

$$X = \frac{V}{V_{eq}(T)} = 1 - exp\left(-fN_rG_r^3t^4\right) \tag{4}$$

where X is the volume fraction of the product phase, V is the volume transformed, $V_{eq}(T)$ is the equilibrium volume amount of the phase at temperature T, f is a shape factor, with a value close to unity, N_r is the nucleation rate, G_r is the growth rate and t is time. For most cases, the volume difference between parent and product phases is small enough that volumes can be interchanged with mol.% values, and V_{eq} in the present work is directly taken from the equilibrium mol.% calculation. The JMA equation can be used to study the transformation of precipitates during aging.

By calculating the JMA equation at different temperatures, the time-temperature-transformation (TTT) diagram can be obtained. Subsequently, it is possible to convert this diagram into a continuous cooling transformation (CCT) diagram using well known additivity rules [22].

2.3. Experimental Procedure

The experimental composition of 2A97 alloy is shown in Table 1.

Table 1. The composition of 2A97 alloy (wt.%).

Alloy	Main Elements			Microalloying Elements			Impurities		
	Li	Cu	Zn	Mg	Mn	Zr	Fe	Si	Al
2A97	1.5	3.8	0.5	0.4	0.3	0.1	0.05	0.03	Bal.

The alloy was prepared by the conventional melting and casting route, and the weight of the ingot was 15 kg. Homogenization was carried out in two steps, of 450 °C and 510 °C, respectively. Subsequently, the ingot was transformed into a plate by hotrolling, using the hot-rolling process as follows. The ingot was heated to 460 °C and then rolled. The temperature of the plate after each pass of rolling was measured. If the temperature was lower than 300 °C, the plate was heated to 460 °C and rolling continued. Finally, solution treatment was performed at 520 °C to prepare for aging.

In this experiment, the samples as cast, homogenized, hot-rolled, and solid-solution were observed by using a JSM 7800F (JEOL Ltd., Tokyo, Japan) scanning electron microscope (SEM). The samples were first roughly ground with 120 #, 400 #, 500 #, and 800 # water abrasive paper, then finely ground with 600 #, 800 #, 1000 #, and 1200 # metallographic abrasive paper, and then mechanically polished. The polished samples were cleaned with an ultrasonic cleaner for 5 min. Finally, the sample surfaces were cleaned with alcohol and blown dry. The microstructure of the sample was observed by backscattered electron signal, and the composition of phases in the alloy were analyzed by a JSM 7800F (JEOL Ltd., Tokyo, Japan) energy dispersive spectrometer (EDS).

3. Results

3.1. The Equilibrium and Solidification Phase Diagrams

The calculated results show that the equilibrium phase of 2A97 Al-Li alloy, as shown in Figures 1 and 2. The main equilibrium phases in the alloy are liquid phase at high temperature, α-Al matrix phase, δ-AlLi phase, θ-Al2Cu phase, T1-Al2CuLi phase, Mg2Si phase, AlMnFe phase and Al3Zr phase. The initial melting temperature of the alloy is 530 °C, which means that the maximum temperature of solid solution cannot exceed 530 °C, otherwise the alloy will overburn, and AlMnFe phase cannot be completely redissolved at

this temperature. In addition, the formation of each phase during solidification was calculated as shown in Figure 3. In addition to the phase in the equilibrium phase diagram, S-Al2CuMg phase also precipitates from liquid phase. This may be caused by element segregation during solidification. Figure 3 shows that the content of crystalline phase is fixed below 490 °C, so the final solidification temperature of the alloy can be regarded as 490 °C. Considering the possible errors in the solidification calculation, the final solidification temperature is conservatively estimated to be 480 °C. Therefore, the ingot cannot be directly heated above 480 °C, otherwise it may lead to overburning.
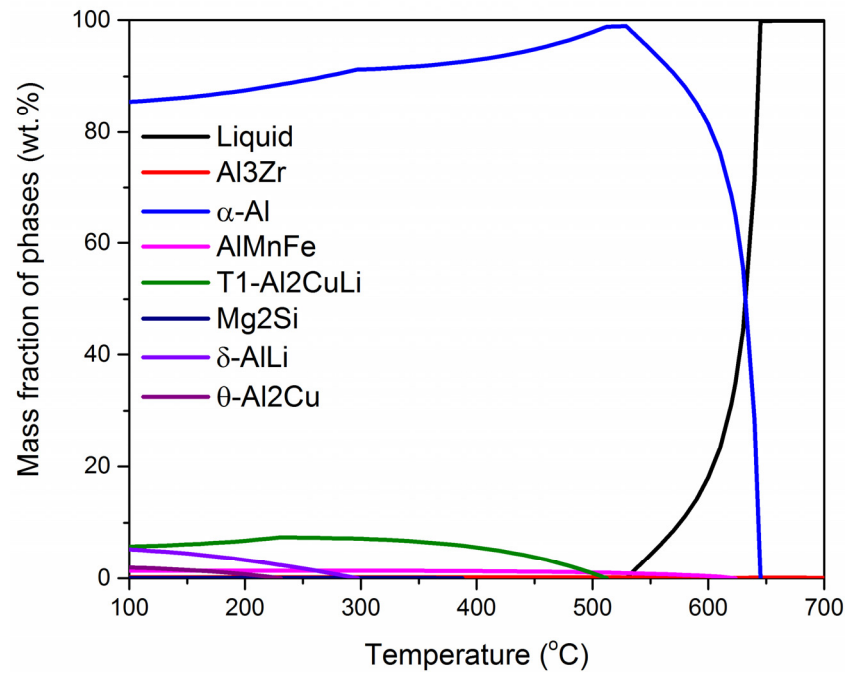
Figure 1. The equilibrium phase diagram of 2A97.
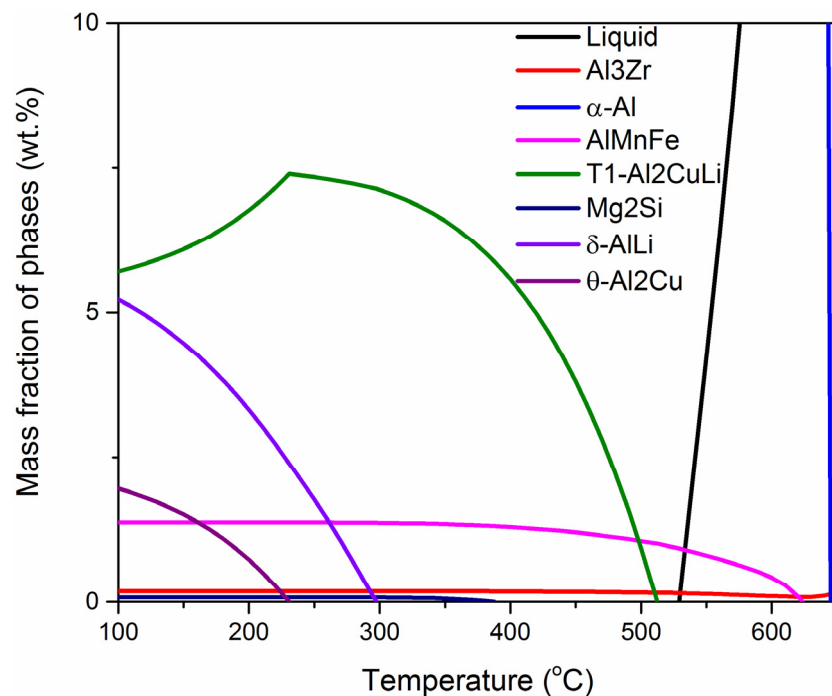
Figure 2. The equilibrium phase diagram of 2A97 (local amplification).
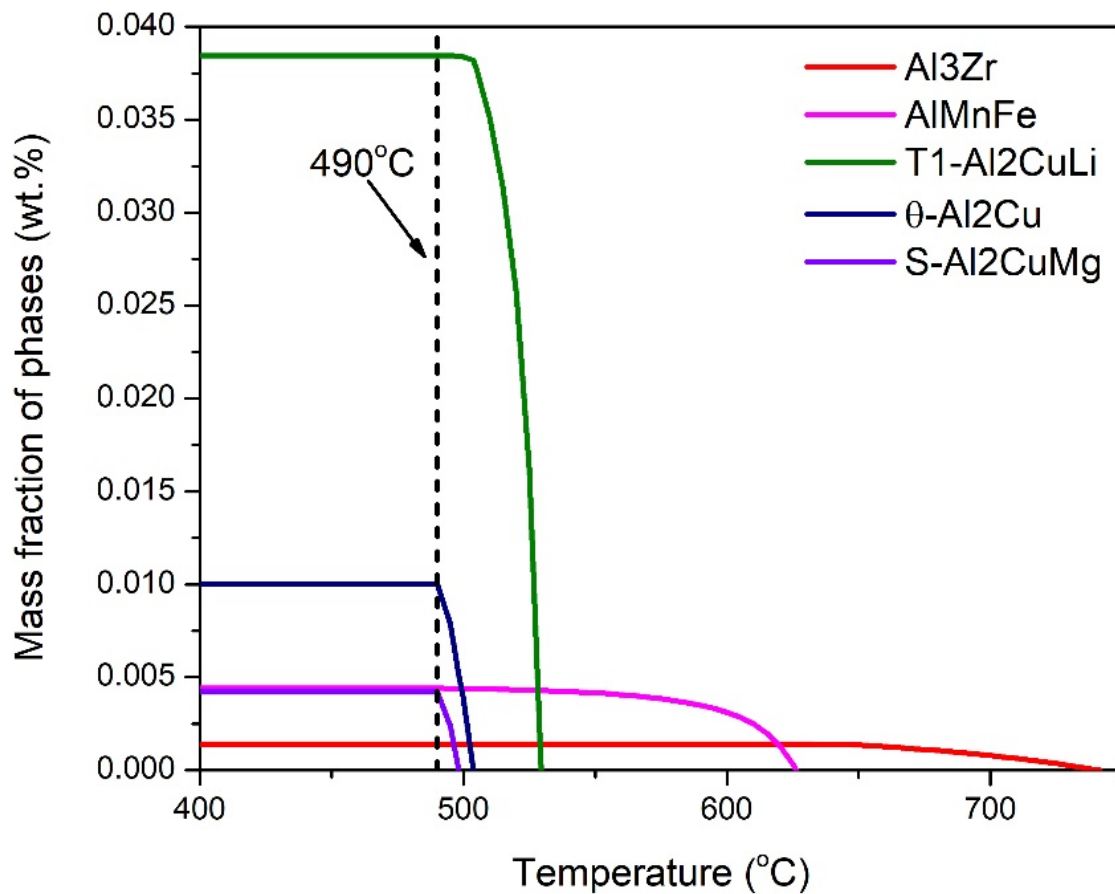
Figure 3. The solidification phase diagram of 2A97 (local amplification).

Figure 4 shows the casting microstructure of 2A97 alloy. Many non-equilibrium eutectic compounds can be seen to be enriched along the grain boundary. This coarse eutectic structure has a low melting point and is fragile, which has a very adverse effect on the hot working properties of the alloy and needs to be eliminated by homogenization.

In order to prevent the alloy from overburning, a safer two-step homogenization process can be adopted. The temperature of the first step is slightly lower than 480 °C (final solidification temperature) to redissolve the low melting point structure and improve the melting point of the alloy. The temperature of the second step is slightly lower than 530 °C (initial melting temperature) to redissolve all phases as much as possible. According to the suggestion, the factory adopteda two-step homogenization process, the first step at 450 °C and the second step at 510 °C. The homogenized microstructure of 2A97 alloy is illustrated in Figure 5. It can be seen that most of the non-equilibrium eutectic compounds have been dissolved.

Figure 6 shows the microstructure of 2A97 alloy after hotrolling. It can be seen that some phases are distributed along the rolling direction [23,24]. According to the EDS results in Table 2, these phases are mainly composed of Al, Cu, Mg, Mn and Fe elements. These are mainly crystalline phases that are not completely redissolved in the homogenization. Therefore, it is inferred from the solidification phase diagram (Figure 3) that these phases may include θ-Al2Cu phase, S-Al2CuMg phase and AlMnFe phase. Many of these coarse brittle compound particles are distributed in the rolled plate. They cannot strengthen the aluminum matrix and are the source of crack initiation, so they reduce the fracture toughness and fatigue performance of 2A97, and need to be eliminated by solid-solution treatment.
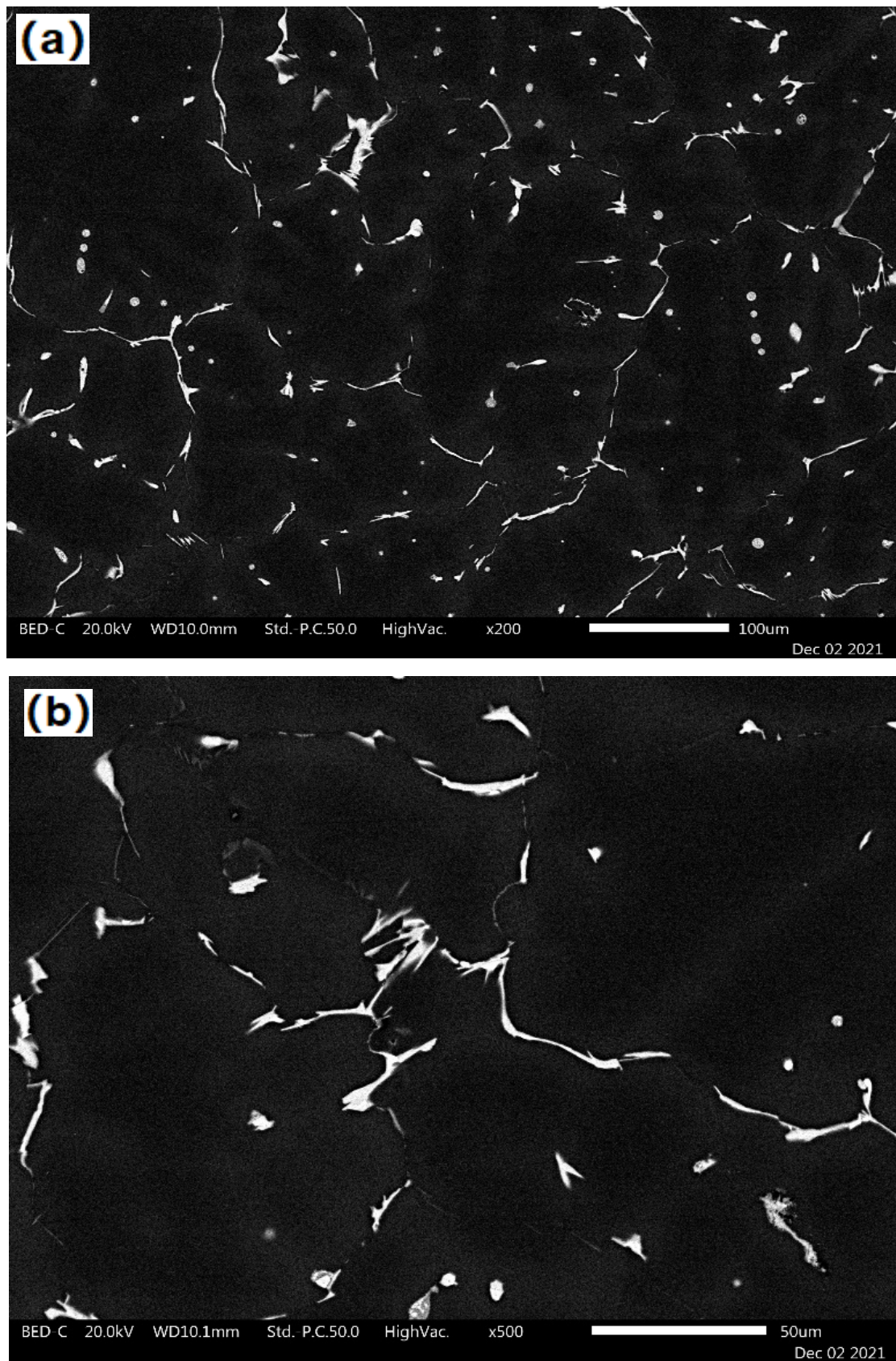
Figure 4. The casting microstructure of 2A97: (**a**) ×200; (**b**) ×500.
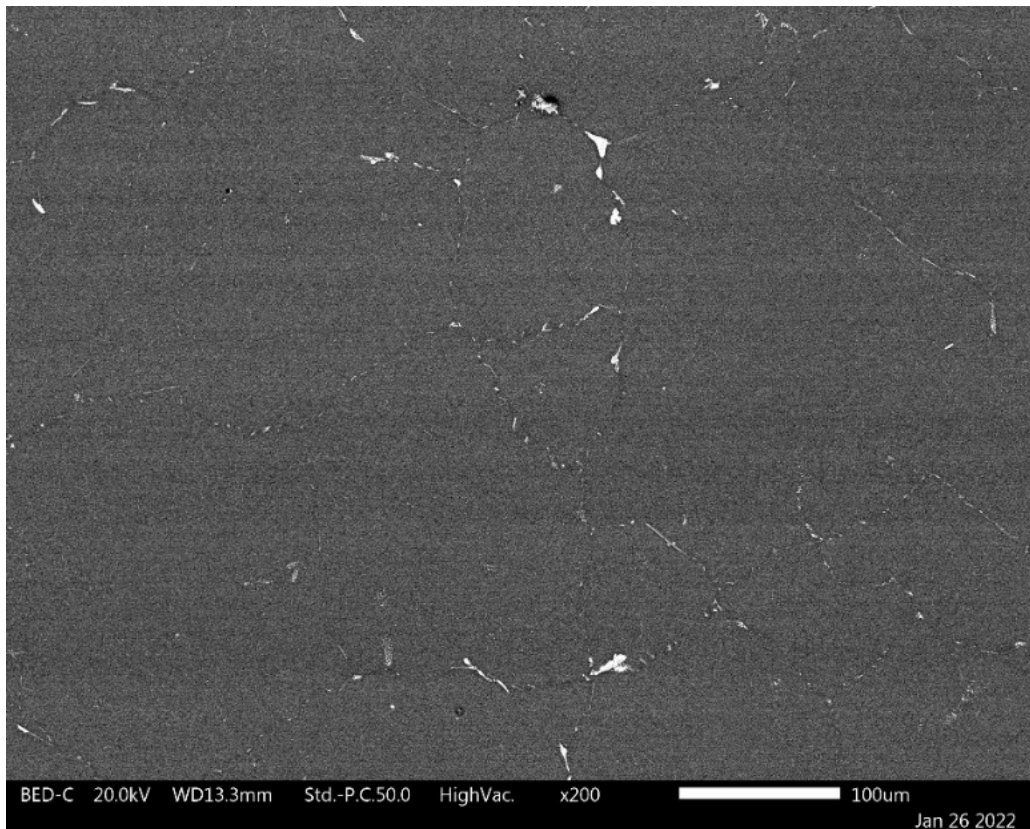
Figure 5. The homogenized microstructure of 2A97.
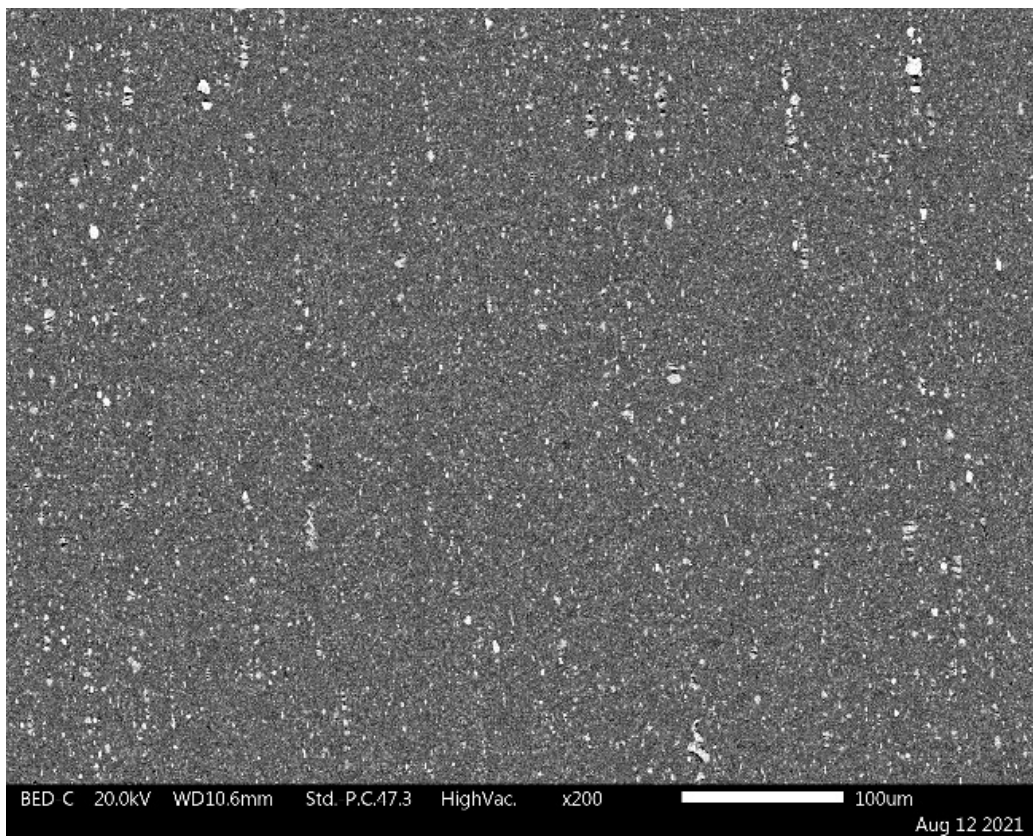
Figure 6. The thermal deformation microstructure of 2A97: (**a**) normal; (**b**) local amplification.

Table 2. The EDS results of the thermal deformation microstructure (wt.%).

	Mg	**Al**	**Si**	**Ti**	**Mn**	**Fe**	**Cu**	**Zn**
1	5.55	39.54	1.39				30.06	
2	2.50	34.37					38.03	
3	1.51	40.00					29.03	
4	4.10	44.84					26.22	
5	3.83	51.52					21.19	
6	2.84	38.54		0.78	2.13	2.65	22.61	1.99
7	2.73	53.96					16.04	
8		58.33					13.66	
9	3.40	45.42					21.03	
10	3.48	53.67					18.58	
11		41.02			2.41	7.55	24.45	
12	3.26	47.93					21.16	
13		46.22			2.12	5.48	19.14	
14	3.18	48.14					20.58	
15		69.52					4.36	
16		72.51					2.60	
17		67.05					11.69	
18		59.41			0.89	2.89	14.30	
19		76.34					2.07	
20		48.07					26.97	
21		65.32					10.30	
22		57.67			2.09	3.97	16.47	

In addition to eliminating brittle particles, the purpose of solid-solution treatment is to dissolve alloy elements such as Cu and Li into the aluminum matrix at high temperature. Then, the supersaturated α-Al matrix was obtained by quenching. The more thorough the solid-solution treatment, the higher the strength that can be obtained by aging. To ensure the alloy elements dissolve into the aluminum matrix as much as possible, the solid-solution temperature should be increased as much as possible on the premise of ensuring that there is no overburning. Therefore, the solid-solution temperature can reach nearly 530 °C (initial melting temperature). According to this suggestion, the factory adopted a higher solid-solution temperature, which reached 520 °C. The solid-solution microstructure and EDS results are shown in Figure 7. It can be seen that only a small quantity of phases is not dissolved. According to the EDS results in Table 3, these phases are mainly composed of Al, Cu, Mg, Mn and Fe elements, and the results are consistent with those of hotrolling. Therefore, it is inferred that these phases may include θ-Al2Cu phase, S-Al2CuMg phase and AlMnFe phase that are not completely redissolved in the solid-solution treatment.

Table 3. The EDS results of solid-solution microstructure (wt.%).

	Mg	**Al**	**Ti**	**Mn**	**Fe**	**Cu**
1	0.85	95.66				3.49
2	2.65	60.97	13.04	3.90	2.54	16.90
3		66.87		2.69	7.45	22.99
4		54.16		5.95	9.35	30.55
5	8.03	57.06				34.91
6		51.93		5.48	9.09	33.50
7		52.91		6.43	11.65	29.01

3.2. The Metastable Phase

The precipitation phase formed during the aging process has the greatest effect on alloy properties in 2A97 [25]. These phases are metastable, except for the T1-Al2CuLi phase, and include δ'-Al3Li and θ'-Al2Cu [26]. The temperature of the solution treatment was set to 520 °C and other equilibrium phases (except α-Al matrix phase) were removed; thus, the metastable phase relationship of 2A97 alloy can be obtained, as shown in Figure 8. It

can be seen that three phases, namely T1-Al2CuLi, δ′-Al3Li and θ′-Al2Cu, appeared in the alloy. When the temperature is lower than 200 °C, θ′-Al2Cu phase increases with decrease in T1-Al2CuLi phase. Subsequently, T1-Al2CuLi, δ′-Al3Li and θ′-Al2Cu were calculated separately and are compared in Figure 9. The stability of T1-Al2CuLi phase is the highest in the aging temperature range of 100 to 200 °C, according to Figures 8 and 9. The relationship of δ′-Al3Li and θ′-Al2Cu (T1-Al2CuLi is removed) is shown in Figure 10. It can be seen that the stability of θ′-Al2Cu is higher than that of δ′-Al3Li. Therefore, the order of stability of the aging precipitation phase is as follows: T1-Al2CuLi phase > θ′-Al2Cu phase > δ′-Al3Li phase. These three phases can precipitate simultaneously in the aging temperature range of 100 to 200 °C.
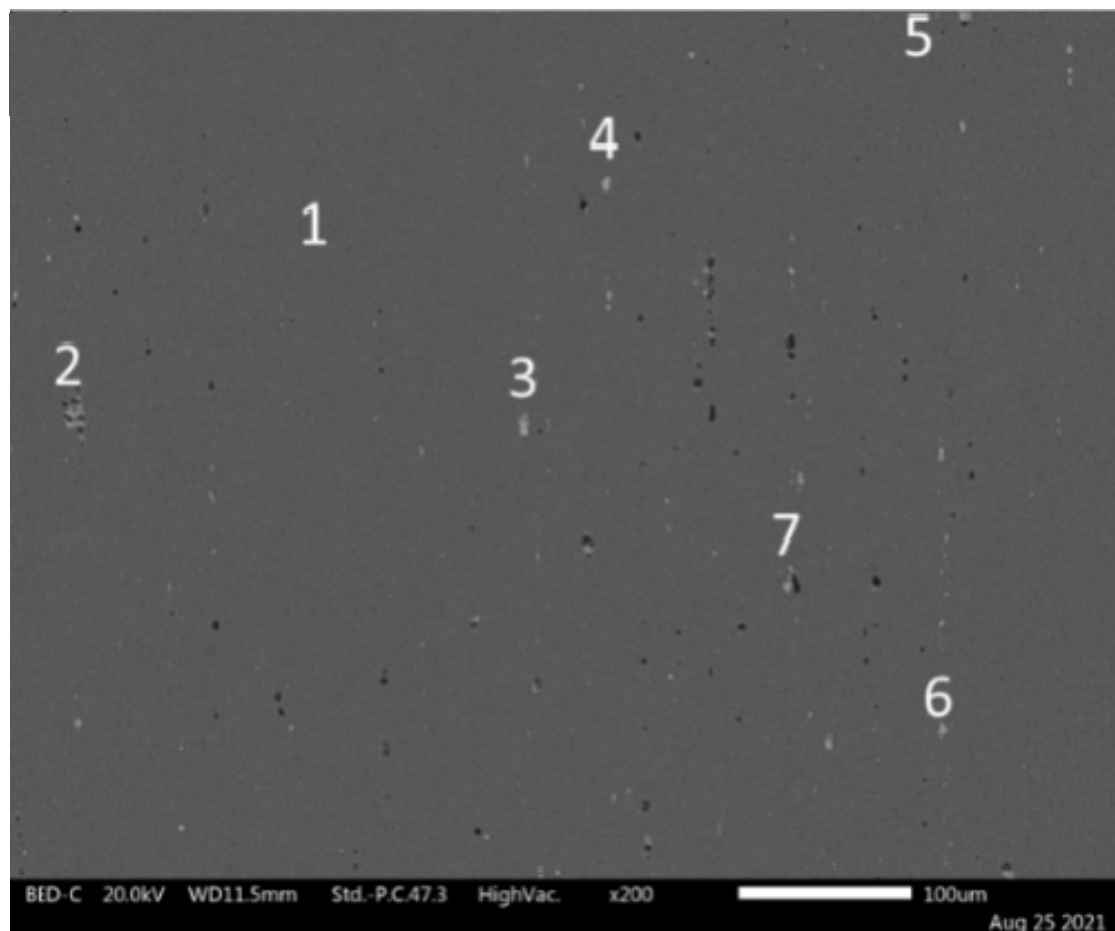
Figure 7. The solid-solution microstructure of 2A97.

Figures 11–13 shows the content of elements in T1-Al2CuLi and metastable phases. It can be seen that the T1-Al2CuLi phase is mainly composed of Al, Cu and Li, and the Al:Cu:Li ratio is close to 2:1:1. Furthermore, there is no big fluctuation in the atomic ratio from high temperature to low temperature. The θ′-Al2Cu phase consists of Al, Cu and Li, and the Al:Cu+Li ratio is close to 2:1, indicating that some Li atoms replace Cu atoms. The δ′-Al3Li phase consists of Al, Zr and Li, and the Al:Zr+Li ratio is close to 3:1, and the content of Zr and Li atoms varies greatly from high temperature to low temperature. When the temperature is higher, the content of Zr and Li atoms is similar, but with the decrease in temperature, the content of Zr decreases, and the content of Li increases. When the temperature is lower than 120 °C, the content of Zr is close to 0, and the δ′ phase is composed of Al and Li elements. This indicates that the effect of Li on δ′-Al3Li is greater than that of Zr when aging below 200 °C.
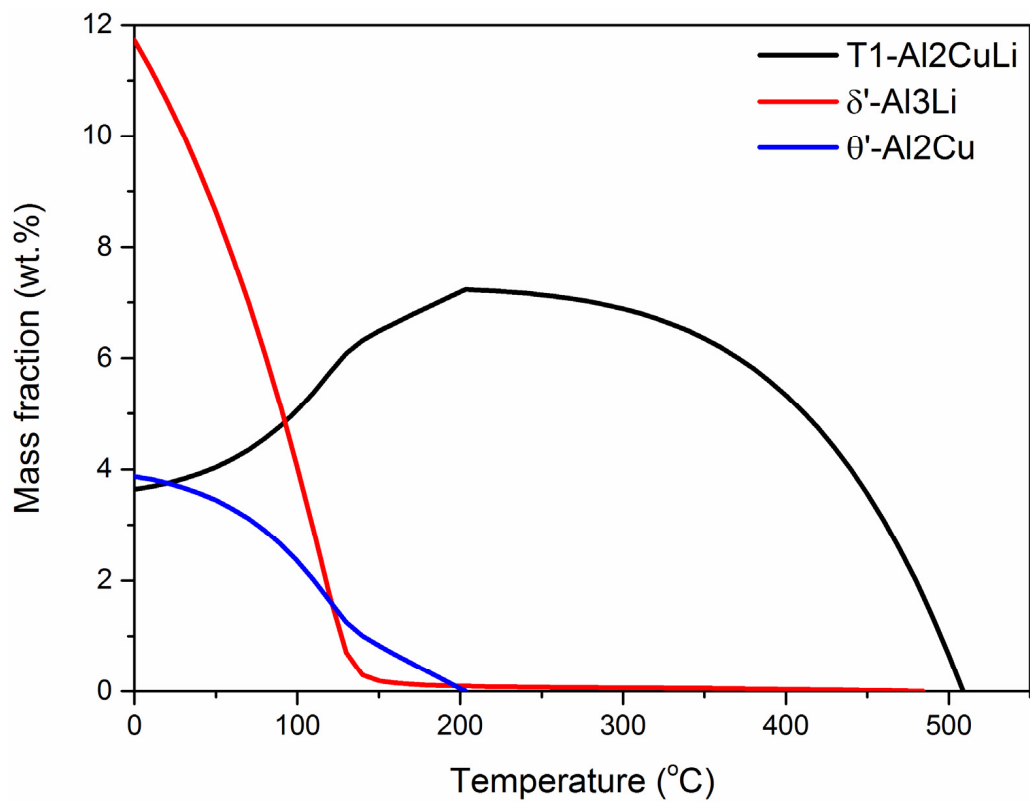
Figure 8. Calculated T1-Al2CuLi, δ′-Al3Li and θ′-Al2Cu phases.
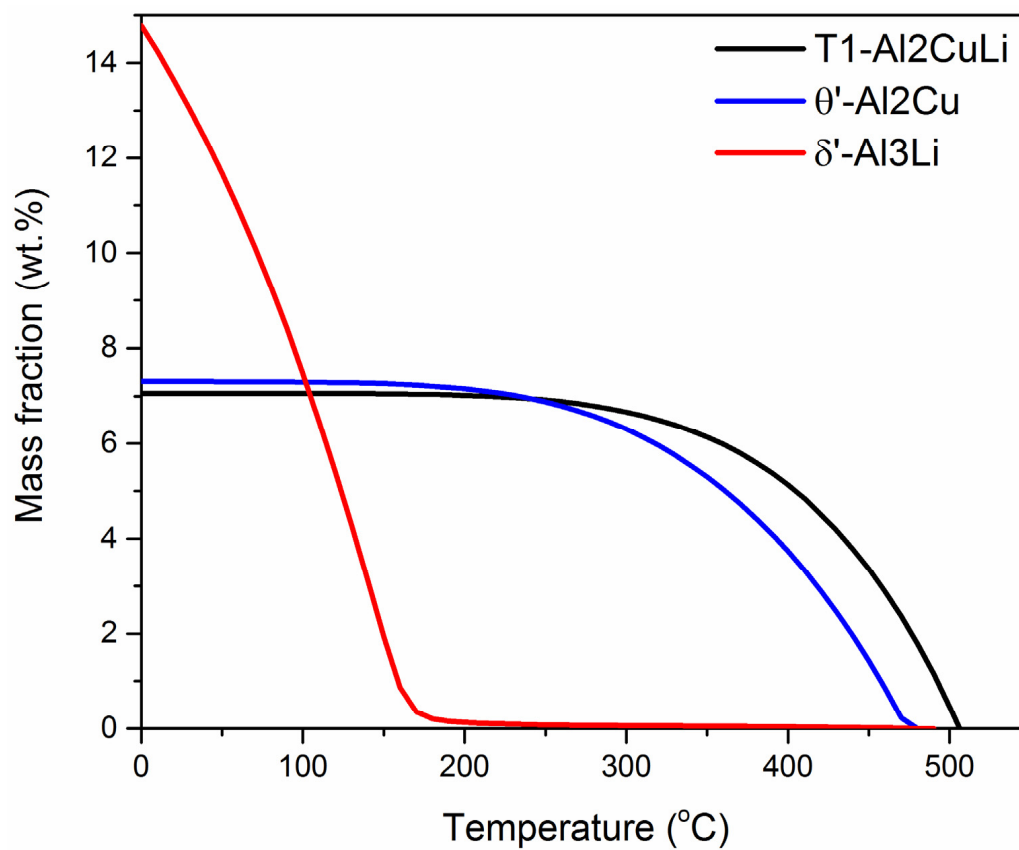
Figure 9. T1-Al2CuLi, δ′-Al3Li and θ′-Al2Cu calculated separately.
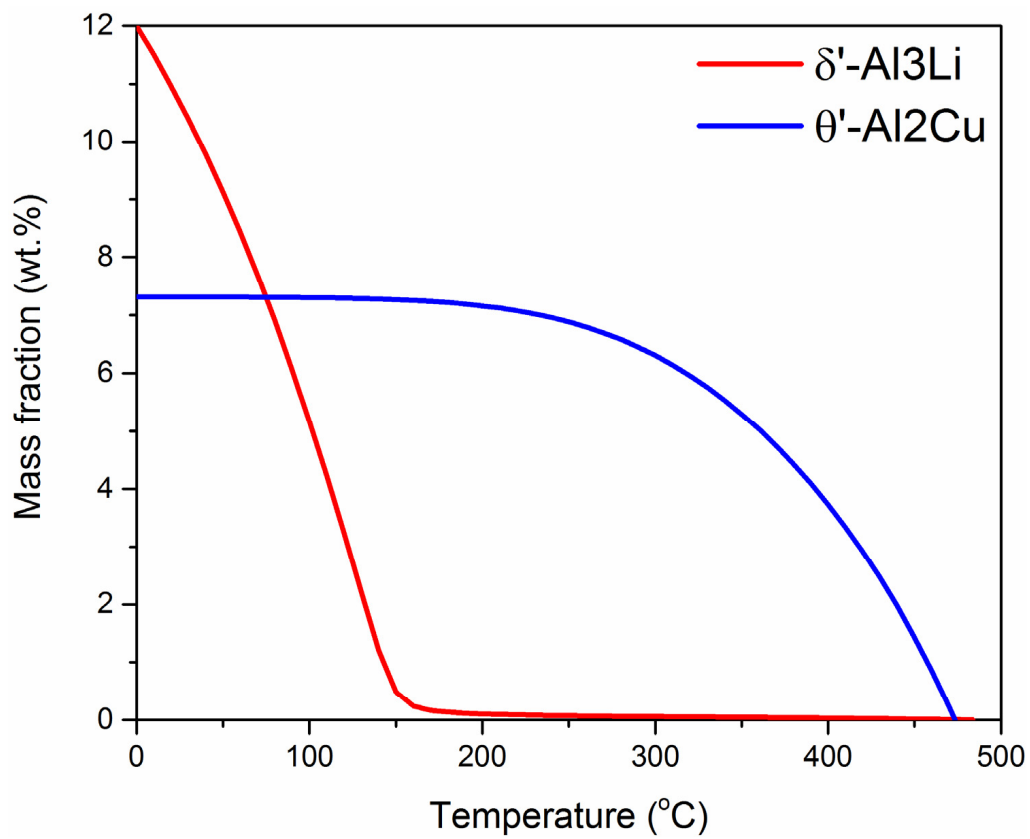
Figure 10. Calculated δ′-Al3Li andθ′-Al2Cu (removed T1-Al2CuLi).
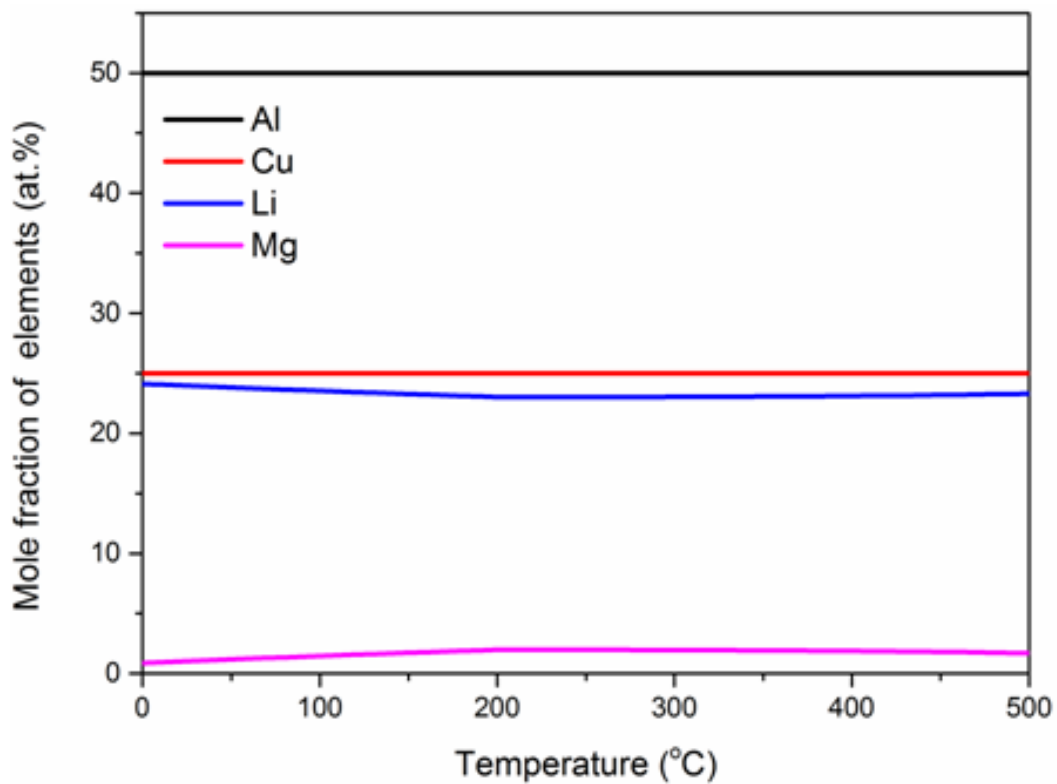
Figure 11. The content of elements in T1-Al2CuLi phase.
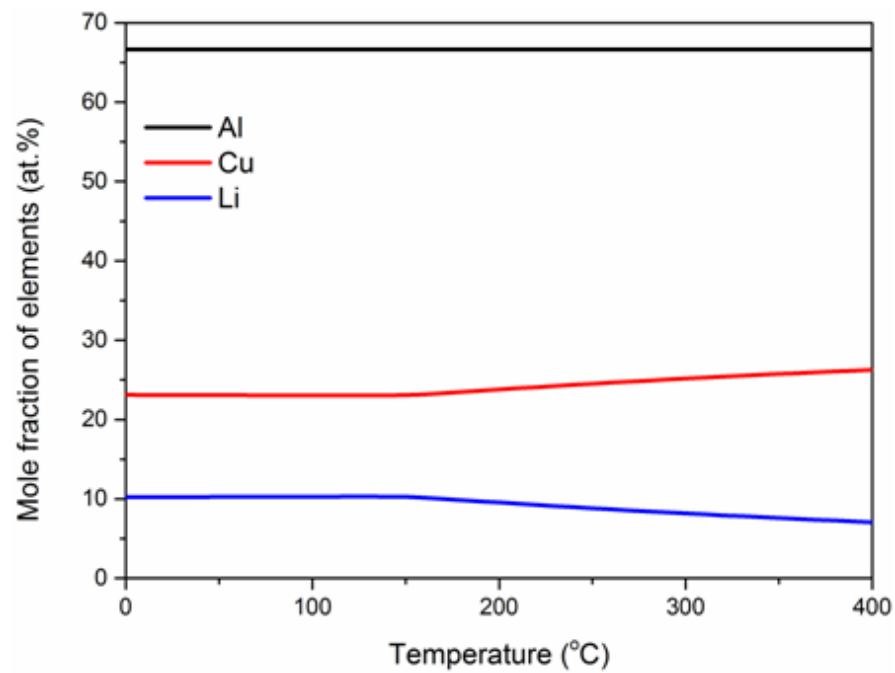
Figure 12. The content of elements in θ'-Al2Cu phase.
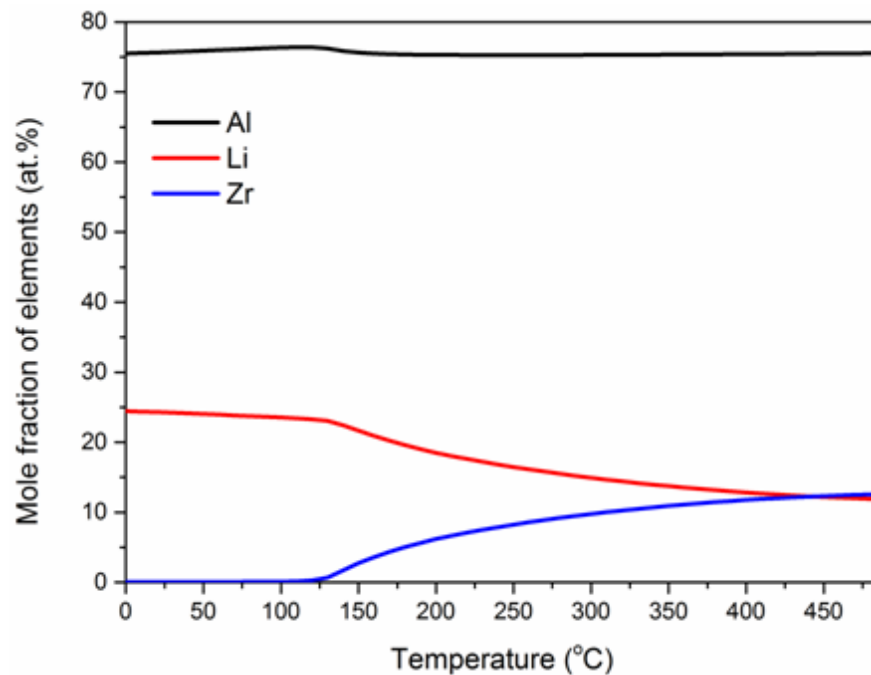
Figure 13. The content of elements in δ'-Al3Li phase.

3.3. The CCT Curves

T1-Al2CuLi phase and metastable phase should not be formed during the cooling of solid-solution, to allow these phases to precipitate during aging. Figure 14 shows the calculated CCT curves of T1-Al2CuLi phase and metastable phases in 2A97 alloy. It can be seen that the initial precipitation temperature of δ'-Al3Li phase is lower than 200 °C, whereas those of T1-Al2CuLi phase and θ'-Al2Cu phase are higher than 400 °C. T1-Al2CuLi phase is located on the leftmost side of figures. This means T1 phase precipitates first in the process of continuous cooling. When the cooling rate is 100 °C/s, the T1 phase can still precipitate, so the precipitation of T1 in the solid-solution cooling process is inevitable. When the cooling rate is 10 °C/s, the precipitation of δ'-Al3Li phase can be avoided, but

when the cooling rate is reduced to 1 °C/s, the phase precipitates during cooling. In summary, a quantity of precipitates will be formed during the solid-solution treatment of 2A97 alloy, which will inevitably result in the loss of the mechanical properties of aging.
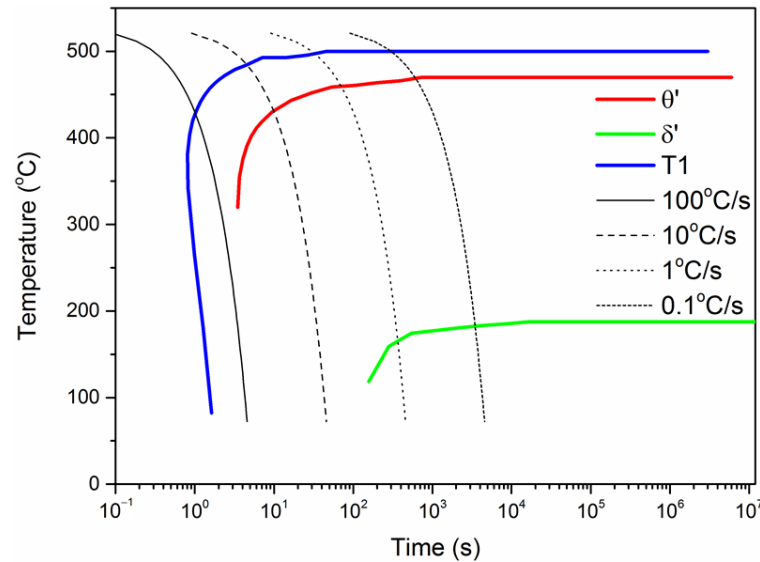
Figure 14. The CCT diagram of 2A97 alloy.

3.4. The Kinetic Curves of Aging

On the basis of the above calculation, the kinetic curves at aging temperatures of 200, 165 and 135 °C were obtained, as shown in Figures 15–17. It can be seen that the main precipitated phases are T1-Al2CuLi phase and θ'-Al2Cu phase at 200 °C. At 165 and 135 °C, δ'-Al3Li phase appears during aging. The total amount of δ'-Al3Li phase increases with the decrease in temperature. In addition, with the decrease in temperature, the total quantity of T1-Al2CuLi and θ'-Al2Cu phases remains almost unchanged, but the precipitation rate of these two phases decreases quickly. Table 4 lists the calculated results and experimental data from refs. [15–17], at different aging temperatures. The calculated results are in good agreement with the experimental data.
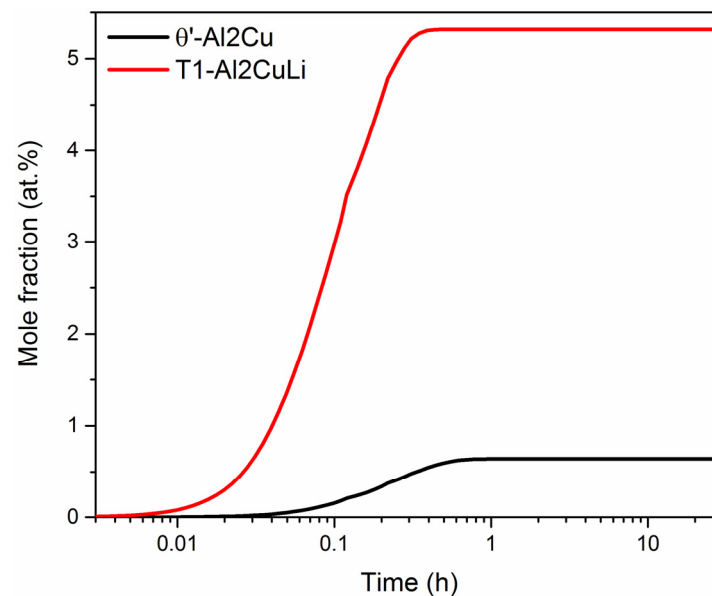
Figure 15. The kinetic curves of 2A97 alloy at 200 °C.
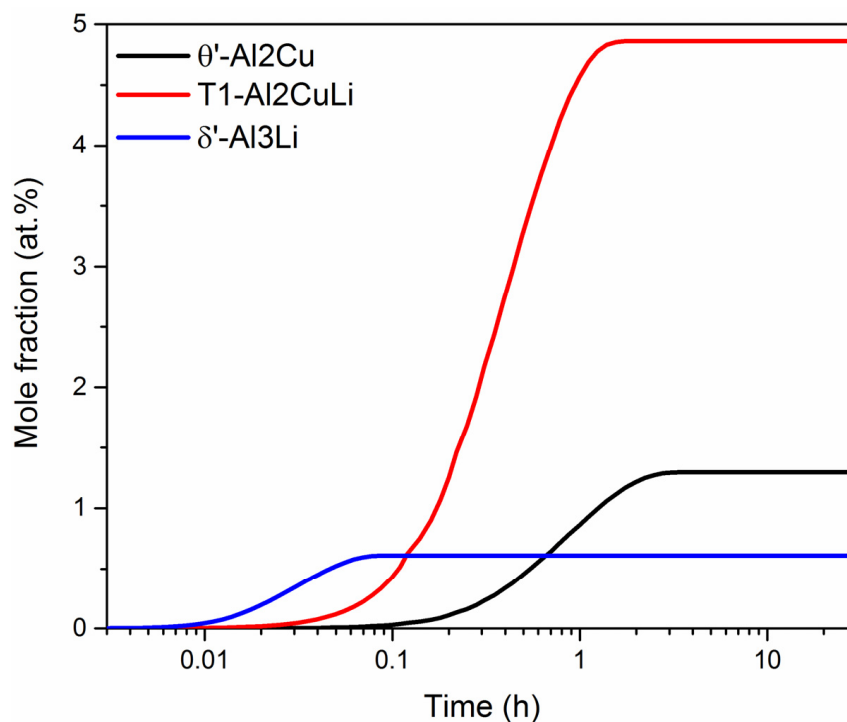
Figure 16. The kinetic curves of 2A97 alloy at 165 °C.
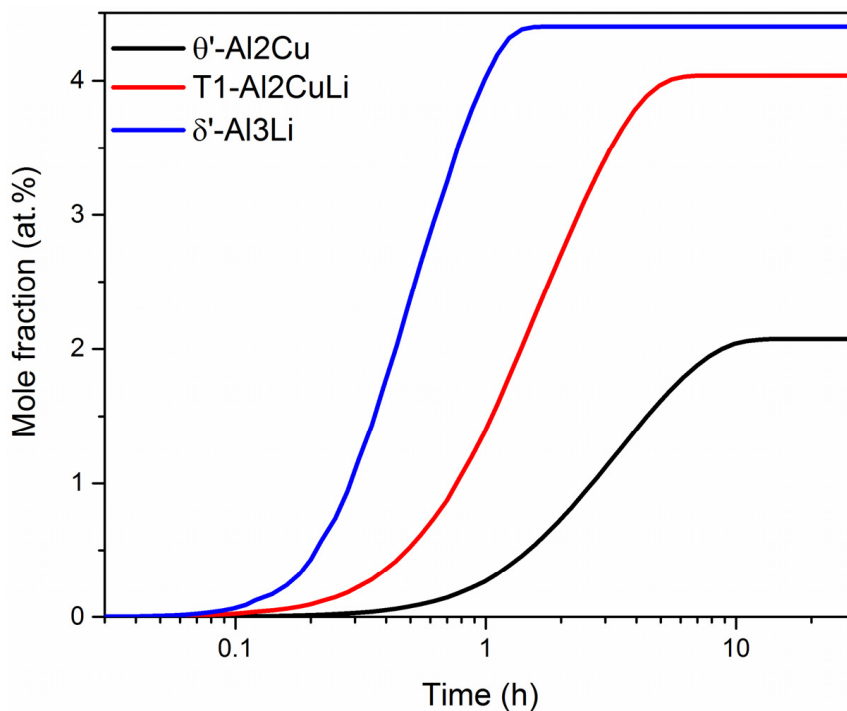
Figure 17. The kinetic curves of 2A97 alloy at 135 °C.

Table 4. Comparison between the calculated results and experimental data.

Aging Temperature	Calculated Results	Experimental Data
200 °C	T1-Al2CuLi and θ′-Al2Cu	T1-Al2CuLi and θ′-Al2Cu [6]
165 °C	T1-Al2CuLi, θ′-Al2Cu and δ′-Al3Li	T1-Al2CuLi, θ′-Al2Cu and δ′-Al3Li [7]
135 °C	T1-Al2CuLi, θ′-Al2Cu and δ′-Al3Li	T1-Al2CuLi, θ′-Al2Cu and δ′-Al3Li [8]

4. Conclusions

In the present study, the Al-Li alloy 2A97was developed using thermodynamic and kinetic methods. The following conclusions were acquired:

(1) According to the experimental composition of 2A97 alloy, the equilibrium phase diagram and solidification phase diagram of 2A97 alloy were calculated by thermodynamic calculation and the SG model.

(2) Referring to the calculated phase diagram, the homogenization temperature was set to 450 °C/510 °C and the solid-solution treatment temperature was set to 520 °C. These results were used in the experiment.

(3) The order of stability of aging precipitation phase is as follows: T1-Al2CuLi phase > θ'-Al2Cu phase > δ'-Al3Li. These three phases can precipitate simultaneously in the aging temperature range of 100 to 200 °C.

(4) δ'-Al3Li phase consists of Al, Zr and Li, and the effect of Li on δ'-Al3Li is greater than that of Zr when aging below 200 °C.

(5) Aging and strengthening phases T1-Al2CuLi, δ'-Al3Li and θ'-Al2Cu will be formed during solid-solution treatment, thus inevitably resulting in the loss of aging mechanical properties.

(6) The main precipitation phases are T1-Al2CuLi phase and θ'-Al2Cu phase at 200 °C. At 165 and 135 °C, δ'-Al3Li phase appears during aging and increases with the decrease in temperature.

Author Contributions: J.W.: calculation and material design. X.X.: experimental verification. All authors have read and agreed to the published version of the manuscript.

Conflicts of Interest: No conflicts of interest were declared during the manuscript submission.

References

1. Starke, E.A.; Staley, J.T. Application of Modern Aluminum Alloys to Aircraft. *Prog. Aerosp. Sci.* **1996**, *32*, 131–172. [CrossRef]
2. Elagin, V.I.; Zakharov, V.V. Modern Al-Li alloys and prospects of their development. *Met. Sci. Heat Treat.* **2013**, *55*, 184–190. [CrossRef]
3. Lequeu, P.; Smith, K.P.; Daniélou, A. Aluminum-copper-lithium Alloy 2050 Developed for Medium to Thick Plate. *J. Mater. Eng. Perform.* **2010**, *19*, 841–847. [CrossRef]
4. Deschamps, A.; Decreus, B.; Geuser, F.D. The influence of precipitation on plastic deformation of Al-Cu-Li alloys. *Acta Mater.* **2013**, *61*, 4010–4021. [CrossRef]
5. Ahmadi, S.; Arabi, H.; Shokuhfar, A. Formation Mechanisms of Precipitates in an Al–Cu–Li–Zr Alloy and their Effects on Strength and Electrical Resistance of the Alloy. *J. Alloys Compd.* **2009**, *484*, 90–94. [CrossRef]
6. Gao, W.L.; Yan, H.; Feng, Z.H.; Lu, Z. Effect of aging treatment on microstructure andmechanical properties of 2A97 Al-Li alloy. *Chin. J. Nonferrous Met.* **2014**, *24*, 1206–1211. [CrossRef]
7. Yuan, Z.S.; Wu, X.L.; Lu, Z.; Xie, Y.H.; Dai, S.L.; Liu, C.S. The Aging Behavior of Aluminum-Lithium Alloy 2A97. *Rare Met. Mater. Eng.* **2008**, *37*, 1898–1901.
8. Yuan, Z.S.; Lu, Z.; Xie, Y.H.; Dai, S.L.; Liu, C.S. Effects of aging treatment on microstructure andproperties of 2A97 aluminum-lithium alloy. *Chin. J. Nonferrous Met.* **2006**, *16*, 2027–2033.
9. Decreus, B.; Deschamps, A.; De Geuser, F. The Influence of Cu/Li Ratio on Precipitation in Al-Cu-Li-x Alloys. *Acta Mater.* **2013**, *61*, 2207–2218. [CrossRef]
10. Rioja, R.J.; Liu, J. The Evolution of Al-Li Base Products for Aerospace and Space Applications. *Metall. Mater. Trans. A* **2012**, *43*, 3325–3337. [CrossRef]
11. Polmear, I.J. Aluminium Alloys—A Century of Age Hardening. *Mater. Forum* **2004**, *28*, 1–14.
12. Dursun, T.; Soutis, C. Recent Developments in Advanced Aircraft Aluminium Alloys. *Mater. Des.* **2014**, *56*, 862–871. [CrossRef]
13. Zhang, S.; Zeng, W.; Yang, W. Ageing Response of Al–Cu–Li 2198 Alloy. *Mater. Des.* **2014**, *63*, 368–374. [CrossRef]
14. Lin, Y.; Zheng, Z.; Zhang, H. Effect of Heat Treatment Process on Tensile Properties of 2A97 Al-Li Alloy: Experiment and BP neural Network simulation. *Trans. Nonferrous Met. Soc. China* **2013**, *23*, 1728–1736. [CrossRef]
15. Chong, G.; Yang, L.; Yu, J. Effect of Thermo-mechanical Treatment Process on Microstructure and Mechanical Properties of 2A97 Al-Li Alloy. *Trans. Nonferrous Met. Soc. China* **2014**, *24*, 2196–2202.
16. Li, H.Y.; Kang, W.; Lu, X.C. Effect of Age-forming on Microstructure, Mechanical and Corrosion Properties of a Novel Al–Li Alloy. *J. Alloys Compd.* **2015**, *640*, 210–218. [CrossRef]

17. Chen, J.; Huang, Z.; Zhang, Y.G.; Chen, C.Q.; Shen, J.Y. Thermodynamic calculation and TEM observation of microstructure of Al-Li-Mg-Si alloys. *Chin. J. Mater. Res.* **2000**, *14*, 271–276.
18. Deschampsa, A.; Siglib, C.; Moureyab, T. Experimental and modelling assessment of precipitation kinetics in an Al–Li–Mg alloy. *Acta Mater.* **2012**, *60*, 1917–1928. [CrossRef]
19. Yoshimura, R.; Konno, T.J.; Abe, E. Transmission Electron Microscopy Study of the Early Stage of Precipitates in Aged Al–Li–Cu alloys. *Acta Mater.* **2003**, *51*, 2891–2903. [CrossRef]
20. Huang, J.C.; Ardell, A.J. Strengthening Mechanisms Associated with T1 Particles in Al-Li-Cu Alloys. *J. Phys.* **1987**, *48*, 373–383. [CrossRef]
21. Li, X.; Saunders, N.; Miodownik, A.P. The coarsening kinetics of γ' particles in nickel-based alloys. *Metall. Mater. Trans. A* **2002**, *33*, 3367–3373. [CrossRef]
22. Kirkaldy, J.S. Diffusion-controlled phase transformations in steels. Theory and applications. *Scand. J. Metall.* **1991**, *20*, 50–61.
23. Kim, S.H.; Lee, H.K.; Yeona, S.M. Selective compositional range exclusion via directed energy deposition to produce a defect-free Inconel 718/SS 316L functionally graded material. *Addit. Manuf.* **2021**, *47*, 102288–102299. [CrossRef]
24. Kim, S.H.; Yeona, S.M.; Lee, J.H. Additive manufacturing of a shift block via laser powder bed fusion: The simultaneousutilisation of optimised topology and a lattice structure. *Virtual Phys. Prototyp.* **2020**, *15*, 460–480. [CrossRef]
25. Zhong, S.; Zheng, Z.Q.; Liao, Z.Q.; Cai, B. Effects of aging treatment on strength and fracture toughness of 2A97 aluminum-lithium alloy. *Chin. J. Nonferrous Met.* **2011**, *21*, 546–553.
26. Yuan, Z.S.; Lu, Z.; Xie, Y.H.; Wu, X.L.; Dai, S.L.; Liu, C.S. Study on Double-Aging of 2A97 Aluminum-Lithium Alloy. *Rare Met. Mater. Eng.* **2011**, *40*, 443–446.